energy&fuels

pubs.acs.org/EF

Article

Single-Droplet Combustion of Jet A-1, Hydroprocessed Vegetable Oil, and Their Blends in a Drop-Tube Furnace

Gonçalo Pacheco,* André Silva, and Mário Costa

Cite This: *Energy Fuels* 2021, 35, 7232−7241

Read Online

ACCESS | Metrics & More | Article Recommendations

ABSTRACT: The environmental impact and the dependence upon fossil fuels in the aeronautical sector have promoted the demand for alternative and greener fuels. The implementation of alternative fuels is one of the main challenges for this sector in the near future. A possible short-term solution might be the blending of biofuels with jet fuel, which would allow for the use of greener fuels and a reduction in the greenhouse gases and pollutant emissions without significant changes in the existing fleets of the companies, with the purpose to develop a "drop-in" fuel. In this context, this work examines the combustion characteristics of single droplets of Jet A-1 (JF), hydroprocessed vegetable oil (NExBTL), and their mixtures in a drop-tube furnace (DTF). The objective of this work is to evaluate the influence of the mixture composition on the fuel characteristics. Droplets with diameters of 155 ± 5 μm, produced by a commercial droplet generator, were injected into the DTF, whose wall temperature and oxygen concentration were controlled. Experiments were conducted for three temperatures (900, 1000, and 1100 °C). The combustion of droplets was evaluated through the images obtained with a high-speed camera coupled with a high magnification lens and an edge detection algorithm. From the images allowed for the analysis of droplet combustion, data are reported for the temporal evolution of droplet sizes and burning rates. The results revealed that the mixtures followed the D^2 law, except the mixture with 75% JF for a DTF wall temperature of 1100 °C. The 75% JF mixture did not follow the D^2 law as a result of the occurrence of puffing and microexplosions, which enhanced the burning rates. Additionally, it was observed that the mixtures with a higher content of JF present brighter flames and higher burning rates.

1. INTRODUCTION

The aeronautical sector had a notorious impact on the emergence of new markets. Consequently, new goods and services became essential in modern-day life. Commercial aviation has become a global business of around 21 450 aircraft currently operating on a single fossil fuel product. The sector is responsible for 2−3% of the global CO_2 emissions, and it is expanding relatively fast with a predicted growth of 4.7% per year, which means that today's fleet will grow to almost 47 990 aircraft by 2037.[1] This rapid growth, coupled with the continuous increase in fuel prices and carbon emissions from this sector (which are expected to grow up to 80%[2]), has inspired intense research on alternative fuels that could supply the sector and reduce the environmental impact.

Biofuels are attractive candidates primarily because of their low greenhouse gas emissions and decreased dependence upon fossil fuel sources.[3] The implementation of biofuels poses a challenge for the aeronautical sector because it requires fuels with high energy density and well-specified properties to comply with the current legislation. Any new aviation fuel must be fully interchangeable with the current jet fuel product to avoid the logistic problems of airports handling multiple fuels of diverse quality and the financial limitations that this would impose.

Because of the long lifecycles of existing infrastructures, aircraft, and engine technologies, a very limited range of applications for new technologies (like the direct use of renewable electricity for electric propulsion), and a need for globally uniform technical and operational standards, it would be too costly to achieve a transition to other low carbon forms of energy supply, such as hydrogen, in the foreseeable future.[4] Besides, given the long-time span to introduce entirely new aircraft designs based on hydrogen into commercial operation of at least 20 years and the limited remaining carbon budget available for the aviation sector, a focus on hydrogen rather than drop-in fuel path would most likely result in significant "waste" of this carbon budget. For these reasons, the main research drive has been around developing "drop-in" fuels for use in the existing fleet because the industry keeps its assets in use for around 40 years[5] as a result of the high investment costs.

However, the use of biofuels raises other concerns. Sustainable aviation fuels must offer low carbon emissions over their lifecycles. The energy crops used as the production source should not challenge food production and ecosystems and not harm the environment.[6] Synthetic paraffinic kerosene from hydroprocessing of esters and fatty acids (HEFA) is also referred to as hydroprocessed renewable jet fuel (HRJ), and

Special Issue: In Memory of Mario Costa

Received: October 16, 2020
Revised: January 14, 2021
Published: January 25, 2021

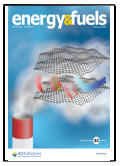

whenever animal biomass is not involved, it is referred to as hydroprocessed vegetable oil (HVO). The hydrodeoxygenation of vegetable oils produces HRJ from animal fats, waste grease, algal oil, and bio-oil, and the primary side products are water and propane.[7] One of the most promising candidates is the HVO called NExBTL, which comes from cellulosic feedstock.[8] This fuel is very promising because it has already been approved for blending with the conventional jet in fuel ratios of 50:50 (vol %) and promotes fewer pollutant formation.

HVO biofuels present a high energy density when compared to regular biodiesel [fatty acid methyl ester (FAME)], which can be used as fuel even without blending.[9] One of the significant advantages of HVO is the potential to reduce the emission of greenhouse gases, such as carbon monoxide (CO), hydrocarbons (HC), nitrogen oxides (NO_x), and particulate matter (PM).[10] HVO is free of aromatics and sulfur and possesses a high cetane number and high thermal stability.[9] Other studies observed that the addition of biofuels reduced the soot formation, primarily because of the reduced aromatic content of the mixture.[11] Additionally, HRJs are highly fit for higher altitude flights as a result of their good cold flow properties. The cold flow properties are a limitation for other biofuels, such as biodiesel and bioalcohol.[9] The characteristics above explained enable the use of HVO in conventional aircraft engines without further engine modification and do not raise any fuel quality issues. However, despite the various benefits mentioned earlier, the use of biofuels also poses substantial concerns. The lack of aromatics in the composition could lead to sealing problems.[11]

Additionally, biofuels usually have higher boiling points and slower gasification rates when compared to conventional fuels. The latter characteristic could lead to various deleterious heterogeneous combustion responses, such as extensive non-premixed burning and causing low combustion efficiency and engine operability problems.[11] Furthermore, biofuels reduced the volumetric energy density, and high production costs (reduction in production costs relies on feedstock availability) make its use not practical for widespread, routine use. These problems can be mitigated through the blending of alternative jet fuels with conventional fuels.[12]

Pratt & Whitney Canada performed several tests in test-bank conditions to assess the impact of HVO on the operability and performance of aviation gas turbines. Engine tests consisted of control, operability, and performance. The fuel type used had little impact on engine performance, and there was no evidence of degradation after the test conclusions. Furthermore, the emission tests of regulated species showed no significant change in the HC, CO, or NO_x emissions compared to jet fuel, 50% HVO, and 100% HVO. The use of biofuel with different chemical compositions and flame characteristics from jet fuel can also contribute to the changes in the NO_x concentration. Much larger reductions were seen in the smoke measurements.[13,14] Aeroméxico, Air China, Air France, Finnair, Iberia, Air France KLM, and Lufthansa have performed commercial passenger flights with hydroprocessed esters and fats.[15] An excellent example corresponds to Japan airlines, which demonstrate the feedstock independence of HRJs through incident-free operating of its Boeing 747-300. The roundtrip test flight operated one of four engines on a 50:50 (vol %) blend of conventional jet fuel and hydroprocessed biomass feedstock. The success of recent test campaigns has highlighted biomass product compatibility with gas turbines and demonstrates the technological readiness and feedstock independence of the hydrotreatment process.[15] The performance of alternative fuels concerning particulate emissions has received considerable attention. Most of the studies that evaluated biomass to liquid (BtL) indicated a reduction in particle matter emissions.

The reduction in the PM emissions could be attributed to the absence of aromatics and a slightly higher H/C ratio for the biofuel compared to Jet A-1.[11,13,16] It is well-established in multicomponent droplet combustion that the droplet tends to violently explode during burning when its components possess vastly different volatilities.[17] This microexplosion event is induced by the superheating of the more volatile components that are diffusionally trapped in the interior of the droplet. The component trapping can appear because, for a liquid element in the droplet interior to be gasified at the droplet surface, it has to first diffuse to the surface. However, liquid-phase mass diffusion is an extremely slow process compared to that of surface regression as the droplet gasifies. Consequently, it could become the rate-limiting process in droplet vaporization.[17] Microexplosions are controlled by the (higher) boiling point of the less volatile component, ultimately leading to an improved combustion performance.[18]

Ma et al.[19] studied the evaporation characteristics of acetone−butanol−ethanol (ABE) and diesel-blended droplets, and the author reported bubble formation and droplet rupture at high ambient temperatures. Puffing/microexplosion causes the fragmentation of droplets, which plays an essential role in improving the atomization. Furthermore, droplets that exhibit strong microexplosion events are characterized by intense and early droplet disruption, which are expected to rapidly lead to complete liquid gasification[20] and improvements in combustion efficiency. The former affirmation is supported by engine experiments that have confirmed the overall benefits of microexplosion in blended fuels.[20−22] Another significant benefit from the blending of different fuels was studied by Shinjo et al.,[23] who also investigated the physics of puffing and microexplosion in emulsion fuel droplets and stated that it might be possible to control microexplosion/puffing in a fuel spray by the appropriate mixing of fuel blends and ambient flow conditions. Wang et al.[24] investigated single-droplet ignition of the miscible mixture in up to 5 atm. The authors found that the increase in pressure favors the occurrence of microexplosions on mixtures that otherwise would not present disruptive burning phenomena, and the microexplosion appears earlier in the lifetime of the droplet. The authors also stated three practical implications of this high-pressure postulate. First, most combustors operate under high pressures. Second, some high-pressure combustors, such as diesel engines and gas turbines, use high-boiling point fuels whose gasification rates can be greatly enhanced with microexplosion. Third, some low-boiling-point fuels that do not microexplode under atmospheric pressure may do so in the realistic high-pressure combustor environment.[24]

The main goal of this work is to study the burning characteristics of the different fuel mixtures, mainly to evaluate the effect of blending different amounts of HVO and jet fuel (JF) in the burning behavior of unsupported free-falling droplets to increase the knowledge on multicomponent fuel combustion. Even though engine studies provide beneficial information regarding fuel performance under realistic conditions, the results observed depend upon several non-controllable variables. Therefore, in a fundamental study, such

https://dx.doi.org/10.1021/acs.energyfuels.0c03476
Energy Fuels 2021, 35, 7232−7241

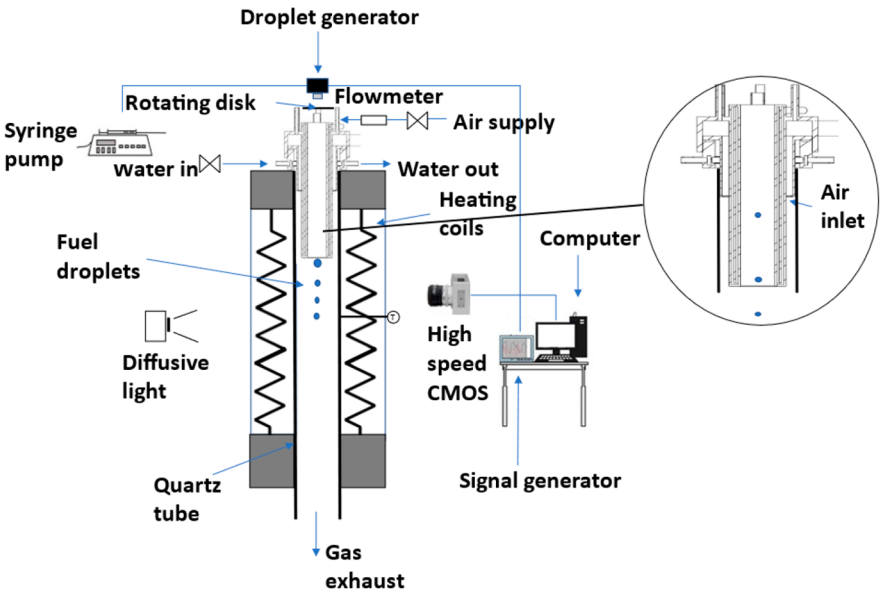

Figure 1. Experimental setup.

as single-droplet combustion, the parameters and test conditions are well-defined. In this way, it is possible to attribute the combustion characteristics observed to the fuel and better comprehend the observed disruptive burning phenomena, such as microexplosions and puffing, and their effect on the droplet diameter evolution and droplet lifetime.

2. MATERIALS AND METHODS

Figure 1 shows the experimental setup used in this study. The drop-tube furnace (DTF) comprises an electrically heated coil and a vertical quartz tube with an inner diameter of 6.6 cm and a length of 82.6 cm. It can achieve wall temperatures up to 1200 °C that are monitored by two type-S thermocouples. The DTF has two opposed rectangular windows, with 2 cm width and 20 cm height, placed in the heating zone, where the coils are located, which is 30 cm long. The image acquisition system (IAS) is positioned perpendicular to the quartz tube in front of rectangular windows. A diffusive light was placed on the opposite side of the IAS, as shown in Figure 1.

Droplets were generated by a TSI device, which produces monosize droplets with the aid of a piezoelectric device. Droplets were produced with an initial diameter of 155 ± 5 μm, an acceptable compromise between actual sizes in practical applications and experimental constraints to obtain reasonable accuracy measurements. The free falling droplet technique permits the use of reduced droplet diameter (while keeping it spherical) symmetry and prevents the formation of microexplosions as a result of interactions of droplet/support fiber.[25] To prevent interdroplet interaction, a minimum distance of 50 diameters between droplets was kept. Droplets travel in a tandem displacement with no sign of interdroplet interaction.

Figure 2 shows the axial temperature profile along the quartz tube for the three ambient conditions (x = 0 cm represents the injector tip). The temperature profile was measured with a fine wire thermocouple (76 μm, type R). When the air enters the quartz tube (x = −20 cm), it is heated and creates a proper environment for the droplet autoignition to occur. The air supply was 5.7 L/min with a precision error of ±2%, to guarantee a stable laminar air flow inside the drop tube, and a series of screens and nets were placed at the air inlet. A detailed description regarding the relation between the droplet and the air flow will be addressed in section 3. The air is heated prior to the droplet injection and is not supplied through the same inlet as the fuel droplets (Figure 1).

This system works with a syringe pump to feed the fuel to the droplet generator and a frequency generator that applies a periodic

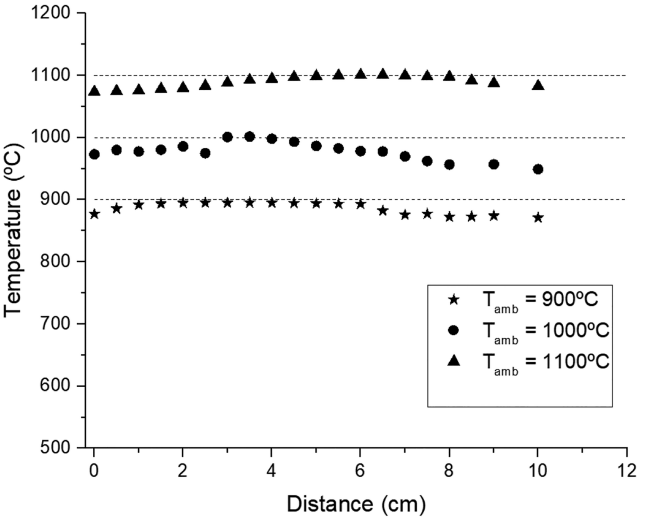

Figure 2. Temperature profile along the quartz tube.

excitation in the form of a square wave. When the excitation frequency is adjusted correctly, the droplet generator produces a steady stream of droplets. For this study, a frequency of 1.5 kHz and a flow rate of 0.8 mL/min was used. A rotating disk with a slot was placed between the droplet generator and the entrance of the injector to increase the interdroplet space. The disk has a diameter of 12 cm and a slot size of 1 × 1 cm and has a rotational speed of 1200 rpm.

Consequently, it was possible to obtain just one droplet per frame and guarantee a single-droplet phenomenon. An essential factor in these experiments is the consistency of droplet sizes. The initial droplet size was obtained, employing several measurements at the exit of the injector tip. The IAS consists of a high-speed CMOS camera connected to a computer, which allows for the control of the camera and stores images for further image data analysis. The camera used was a CR600 × 2 from Optronics. A frame rate of 1000 fps was used, coupled with a resolution of 1280 × 500 pixels. This frame rate was used because a further increase would mean a reduction in the resolution size of the images, and to produce accurate results, the image should be as wide as possible because it allows for a better analysis of the behavior of droplets. A high-magnification lens (Zoom 6000 lens system) was attached to the high-speed camera. This

https://dx.doi.org/10.1021/acs.energyfuels.0c03476
Energy Fuels 2021, 35, 7232−7241

modular system permits the magnification of a traditional microscope at a working distance of 300 mm. It is composed of 6.5× zoom, 12 mm full-frame (FF), a 0.25× lens attachment, and a 2.0× short adapter, with a magnifying range of 0.35−2.25, leading to an increase in the spatial resolution of the image up to 8.2 μm/pixel.

The setup required homogeneous background illumination to intensify the contrast and to improve the quality of the images. To provide uniform illumination, a diffusion glass was placed in front of the light-emitting diode (LED) projector. Calibration of the IAS was performed before every set of measures with a reference with 76 μm diameter (composed of a platinum wire) that was placed in the focal plane. Subsequently, the scale micrometers per pixel was determined for the treatment of data. Figure 3 shows a 100% JF droplet burning at 1100 °C. This imaging method gives information about the droplet size and motion and the flame location. In this work, ignition was considered to occur when 15% of the maximum pixel luminosity was reached.

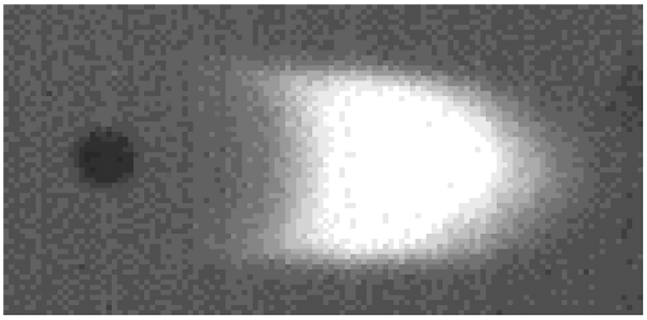

Figure 3. 100% JF droplet burning at 1100 °C.

The procedure used to obtain results, such as burning/evaporation rates, was as follows. The droplet diameter was automatically calculated using an edge detection algorithm and then treated to obtain the previously referenced parameters. To determine the droplet outline, both the brightness difference between the lighter background and the darker droplet in Figure 3 and the local gradient of brightness were considered. The brightness gradient was determined using the four connected pixels in the vertical and horizontal axes. Both the brightness difference and brightness gradient were calculated for each pixel in each image containing a droplet. There was a sharp transition from light gray to darker gray pixels near the surface of the fuel droplet. A pronounced gradient of brightness values characterizes the outline region. For each experimental condition, a minimum of 30 single droplets was analyzed. The measurements present less than 4% uncertainty for calculating the droplet velocity along the quartz tube, a diameter uncertainty of less than 9%, and an uncertainty of less than 11% for the burning rate.

2.1. Fuel Characterization. Jet A-1, HVO (NExBTL), and their blends used in this study were made with the aid of a volumetric pipet. The pipet has a volumetric capacity of 50 ± 0.05 mL. Subsequently, the mixtures were stored in closed glass recipients to preserve their properties. Table 1 shows the main properties of the fuels used. These measurements were obtained from the fuel suppliers and in previous works.[26]

3. RESULTS AND DISCUSSION

3.1. Droplet Characterization. The Reynolds number is an important dimensionless number to characterize the flow regime. The air properties were taken from the international standard atmosphere (ISA), and the droplet velocity and diameter were measured using the IAS. On the basis of these properties, the average droplet velocity relative to the air flow was calculated. Consequently, the mean flow velocity was determined for each condition. Table 2 shows the air properties for different conditions. With the air properties defined, it is possible to calculate the mean air velocity and Reynolds number inside the quartz tube for each condition, with the quartz tube diameter being used as the characteristic linear dimension. Table 3 shows that the Reynolds number (Re) in the quartz tube is relatively low, meaning that it should have a low turbulent intensity and provide a stable test atmosphere. Table 3 shows the Reynolds number relative to the air flow for the droplets entering the quartz tube (Re_D). It is possible to calculate their mean droplet Reynolds number (Re_D) through the air properties, droplet diameter, and velocity. From this analysis, it can be seen that, as the temperature increases, the Reynolds number reduces. The

Table 2. Air Properties for Each Operating Condition

	900 °C	1000 °C	1100 °C
air density (kg/m^3)	0.30	0.27	0.25
dynamic viscosity (Pa s)	45.6×10^{-6}	47.88×10^{-6}	50.01×10^{-6}

Table 3. Flow Properties for Each Condition

	air flow velocity (m/s)	Re	Re_D
900 °C	0.11	47.0	0.6
1000 °C	0.12	44.8	0.5
1100 °C	0.12	42.8	0.4

Table 1. Fuel Properties

parameter	100% JF	75% JF	50% JF	25% JF	no JF
density at 20 °C (kg/m^3)	798	794	789	785	780.6
viscosity at 40 °C (mm^2/s)	1.2	1.9	2.3	2.5	2.98
aromatics (wt %)	13.8	10.4	7.0	3.5	0.2
distillation at 10 vol % (°C)	169.9				262
final boiling point (°C)	237.2				300
sulfur (wt %)	0.3	0.225	0.15	0.075	≈0
cloud point (°C)	−26				−30
LHV (MJ/kg)	43.4	43.5	43.6	43.8	43.9
LHV (MJ/L)	34.6	34.5	34.4	34.3	34.2
hydrogen content	14.5				15.4
carbon content	85.5				84.6
H/C ratio	1.99				≈2.18
average chemical composition	$C_{10.8}H_{21.8}$				$C_{15}H_{32}$−$C_{18}H_{38}$

https://dx.doi.org/10.1021/acs.energyfuels.0c03476
Energy Fuels 2021, 35, 7232−7241

reduction is due to variations in the air properties (dynamic viscosity and density) caused by the temperature increase.

To calculate the droplet velocity, the centroid position for two sequential frames of a droplet is considered and the distance between them is divided by the time between the two frames (0.001 s). Figure 4 shows the droplet relative velocity to

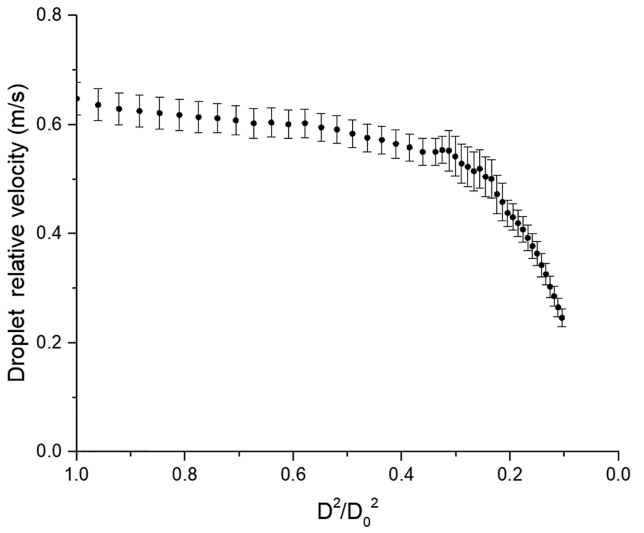

Figure 4. Droplet velocity profile as a function of the diameter.

the gas as a function of the droplet diameter. Droplets entered the quartz tube with a nearly constant relative velocity of approximately 0.63 m/s. The relative velocity between droplets and the hot flow was very low; hence, the droplet Reynolds number (Re_D) will also present a low value (Reynolds number based on the droplet velocity in relation to flow) of <1 for the whole droplet history, more concretely ≤0.6 for the case with the highest Re_D. Droplets burn in a laminar stable atmosphere that did not influence the trajectory of the droplets and guaranteed that droplets would travel in the central axis of the quartz tube. The combination of these effects with the small droplet sizes in use allows for the creation of spherical droplets, necessary for the precise evaluation of the droplet diameter evolution.

3.2. Combustion Behavior of the Single Droplets.

Figures 5−7 show sequences of instantaneous images of burning droplets at different temperatures and instants. After droplets enter the combustion chamber, they are ignited as a result of the high air temperature and a flame is established at the wake of each droplet. The moment when the droplet ignites is assumed to be t = 0 ms. The figure also reveals that the flame intensity (luminosity) decreases and the droplet lifetime increases as the ambient air temperature decreases from 1100 to 900 °C (Figures 5−7), regardless of the composition of the fuel mixture.

In particular, the flame intensity increases as the percentage of Jet A-1 in the fuel mixture increases. Interestingly, the disruptive burning phenomenon of the fuel mixture was observed with 75% Jet A-1 (Figure 5). At t = 16 ms (Figure 5), a sudden increase in the flame size and intensity occurs. This phenomenon, often called puffing, is characterized by the release of volatiles as a result of the breakup of an expanding gas bubble formed inside the fuel droplet. This event is followed by a rapid decrease in the diameter of the droplet, as seen at t = 24 ms. These observations are consistent with other

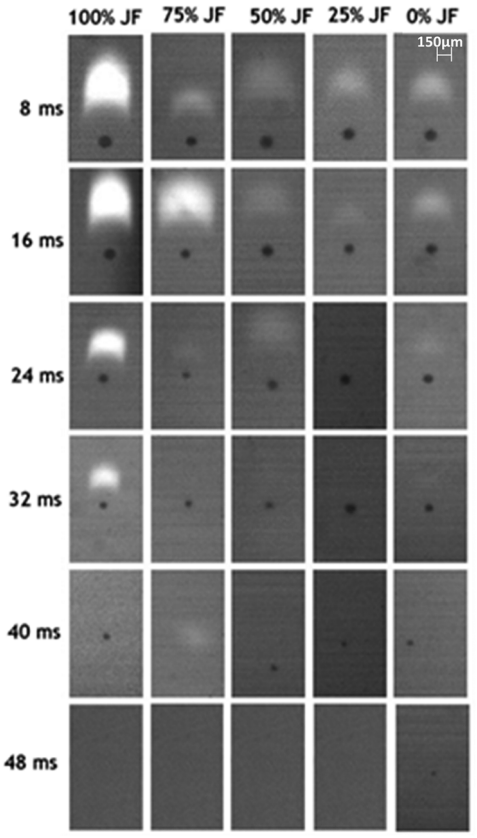

Figure 5. Sequences of instantaneous images of burning droplets at 1100 °C.

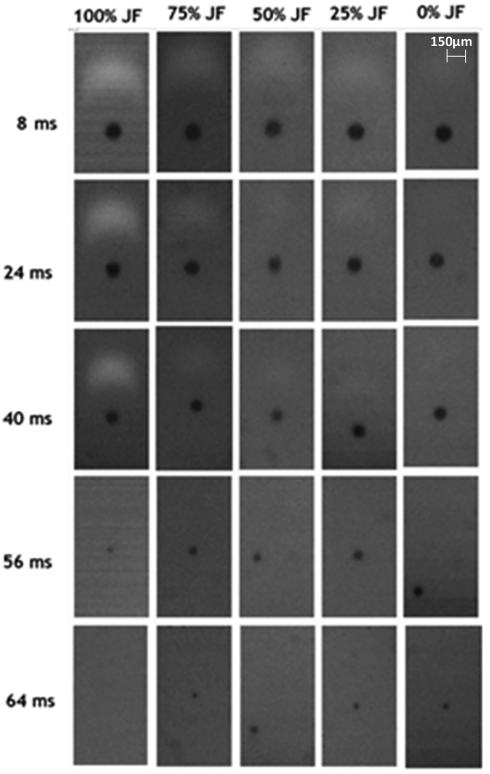

Figure 6. Sequences of instantaneous images of burning droplets at 1000 °C.

https://dx.doi.org/10.1021/acs.energyfuels.0c03476
Energy Fuels 2021, 35, 7232−7241

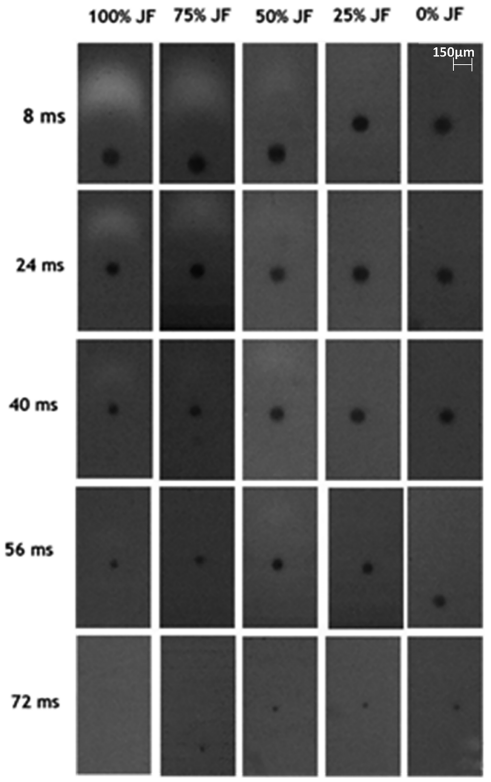

Figure 7. Sequences of instantaneous images of burning droplets at 900 °C.

studies.[12] The occurrence of puffing precedes microexplosions, as observed at t = 40 ms, with the establishment of a spherical flame and no visible droplet. The occurrence of microexplosions significantly reduces the droplet lifetime. It is evidenced that disruptive burning processes occur in a brief time interval, such as the microexplosion, which is stated to occur in less than 200 μs.[27] It suggests that the imaging rate should be higher than 5000 frames per second to track every step of the phenomena properly. Therefore, at the frame rate used in these experiments, it is impossible to observe in detail every step fully detailed of the microexplosion and puffing.[27]

3.3. Occurrence of a Microexplosion. In this section, the discussion of microexplosions will be addressed in a more detailed analysis. Table 4 characterizes the microexplosions

Table 4. Characterization of Microexplosions for the Fuel Mixture with 75% Jet A-1 at 1100 °C

	microexplosions	normal combustion
probability (%)	71	29
droplet diameter range at the microexplosion instant (μm)	55−70	

regarding their probability of occurrence. Additionally, droplet diameters immediately before the microexplosion will also be compared. It is seen that microexplosions occurred for 71% of the droplets for the fuel mixture with 75% Jet A-1 at 1100 °C (cf. Figure 5). This phenomenon does not occur for every droplet. A high puffing intensity in the earlier stages of droplet combustion might be the reason for the suppression of microexplosions, and the primary gas bubbles have already broken up and released the most volatile components in the mixtures. Microexplosions occurred for droplet diameters comprised between 55 and 70 μm. Microexplosions are a stochastic phenomenon that depends upon various factors that can influence their occurrence. The occurrence range for microexplosions depends upon several factors, such as the variation in the initial droplet size, the fuel mixture composition, and the previous appearance of puffing. It should be pointed out that, if puffing or microexplosion occurs, secondary atomization will be induced. Generally, secondary atomization enhances droplet evaporation and fuel/air mixing,[23] reducing the droplet lifetime and improving combustion efficiency. Even though secondary atomization presents great potential for improving the atomization of liquid fuels, the understanding of disruptive phenomena is far from sufficient. Therefore, further studies are necessary to improve the knowledge of the disruptive combustion characteristics of fuel blends for a better and further implementation of biofuels.[18]

3.4. Droplet Size Evolution and Burning Rate. The analysis below is based on the well-known D^2 law. Figures 8−10 show the normalized droplet diameter as a function of

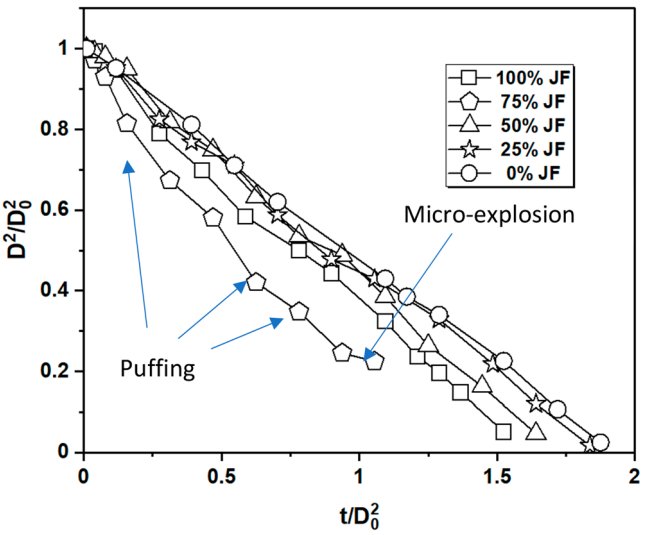

Figure 8. Normalized droplet diameter as a function of the normalized time at 1100 °C.

the normalized time for the three different temperatures studied. It is seen that, after an initial heating period, droplet size evolution obeyed the D^2 law, which predicts that the normalized square diameter decreases linearly with a nearly constant slope, the so-called burning rate, k. The normalization process is performed by dividing both the squared diameter and the time by the initial squared droplet diameter (D_0^2). Moreover, the normalized droplet diameter evolution is quite similar for all conditions, except for the fuel mixture with 75% Jet A-1 at 1100 °C (Figure 8) that presented disruptive burning phenomena. The droplets of pure HVO present the longest burning time, and the droplets of pure Jet A-1 present the shortest burning time. The differences in the burning times can be attributed to the volatility differences of these fuels and as a result of the reduced reactivity of HVO in comparison to Jet A-1. The evolution of the droplets of the fuel mixture with 75% Jet A-1 shows the most distinctive behavior because of the occurrence of puffing and microexplosions. Its diameter evolution curves present instabilities (discrete diameter

https://dx.doi.org/10.1021/acs.energyfuels.0c03476
Energy Fuels 2021, 35, 7232−7241

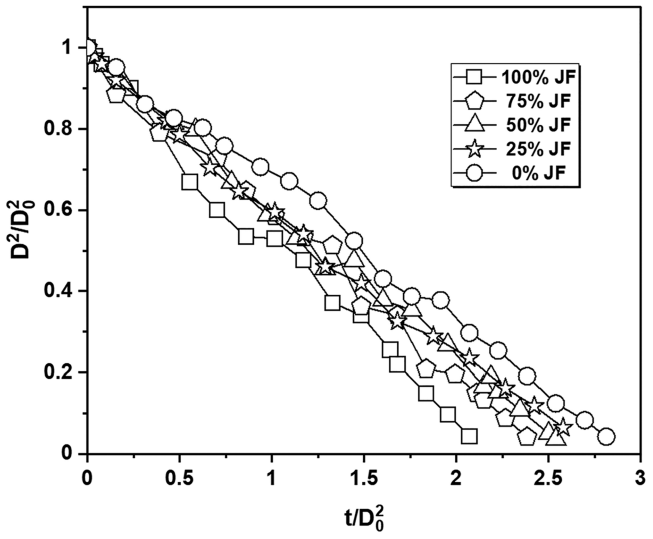

Figure 9. Normalized droplet diameter as a function of the normalized time at 1000 °C.

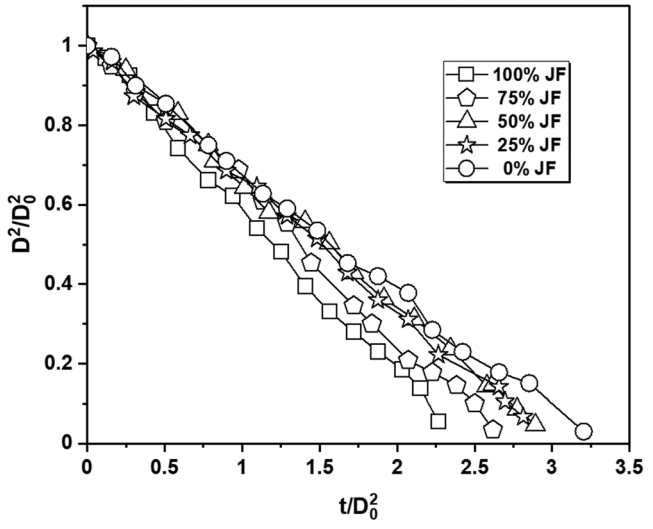

Figure 10. Normalized droplet diameter as a function of the normalized time at 900 °C.

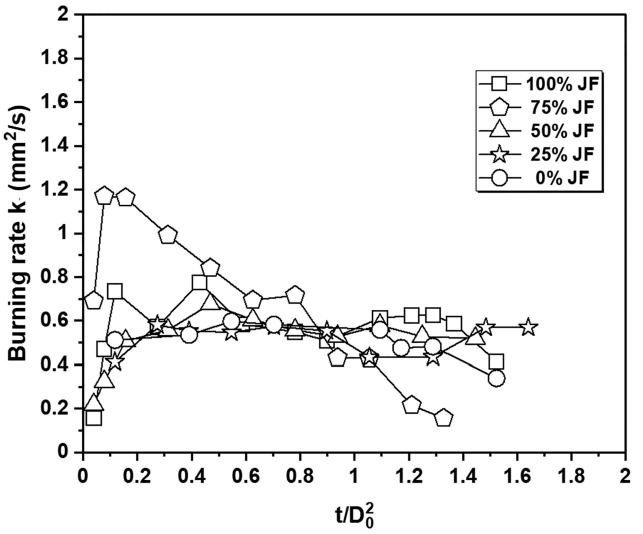

Figure 11. Droplet burning rate as a function of the normalized time at 1100 °C.

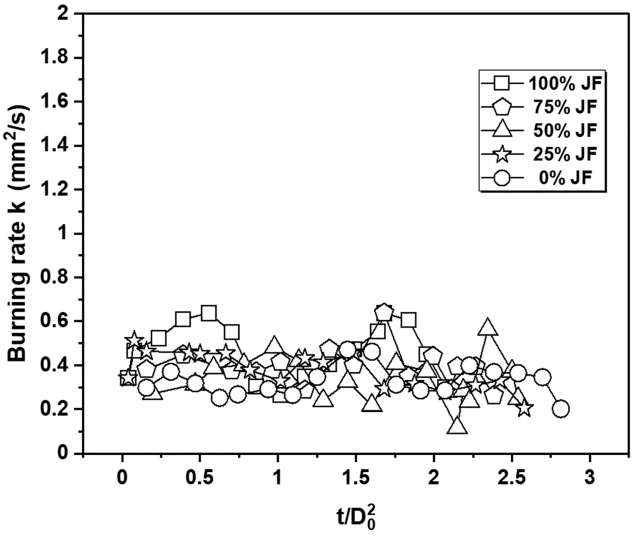

Figure 12. Droplet burning rate as a function of the normalized time at 1000 °C.

variations) as a result of the ejection of volatiles inside the droplet.[28] According to the literature, it can be theorized that, after the heating period is achieved and the flame is established, the gasification is sustained by the co-vaporization of different components.[11] During this process, some of the most volatile components remain trapped inside the core of the droplet as a result of liquid-phase diffusional resistance and could become superheated, leading to the nucleation of gas bubbles and the subsequent violent rupturing of the droplet in the form of puffing or microexplosions. Finally, Figures 8−10 reveal that the burning time increases as the air temperature decreases for all of the mixtures. The increase in the environmental temperature leads to the enhancement of the heat transfer from the environment to the droplet, improving the evaporation process and, consequently, increasing its burning rate.

The burning rates were calculated to obtain further insight into the behavior of burning droplets for each blend in different conditions. Figures 11−13 show the burning rate as a function of the normalized time at different temperatures. The burning rates were calculated from the data presented in Figures 8−10 and follow the procedures described by Muelas et al.[29] The burning rate was determined by calculating the instantaneous slopes of the curves. The D^2 curve slope represents the burning rate, $K = -\mathrm{d}(D^2)/\mathrm{d}t$. This method raises a problem because derivation greatly increases any experimental uncertainties and instabilities, and similar to other authors, a three-point moving average was employed in both the burning rate graphics and the D^2 evolutions to smoothen the curves.[29] This curve presents an apparent unsteady behavior, even though the D^2 curves present a strong linear tendency. Except for the fuel mixture with 75% Jet A-1 at 1100 °C (Figure 11), all droplets present a similar burning behavior, with an initial rapid increase in the burning rate. At the initial droplet combustion period, the amount of fuel that evaporates is reduced as a result of the low initial temperature of the droplet, resulting in a lower burning rate. The increase in the burning rate, coupled with the increase in droplet temperature, is followed by an almost constant evolution of

https://dx.doi.org/10.1021/acs.energyfuels.0c03476
Energy Fuels 2021, 35, 7232−7241

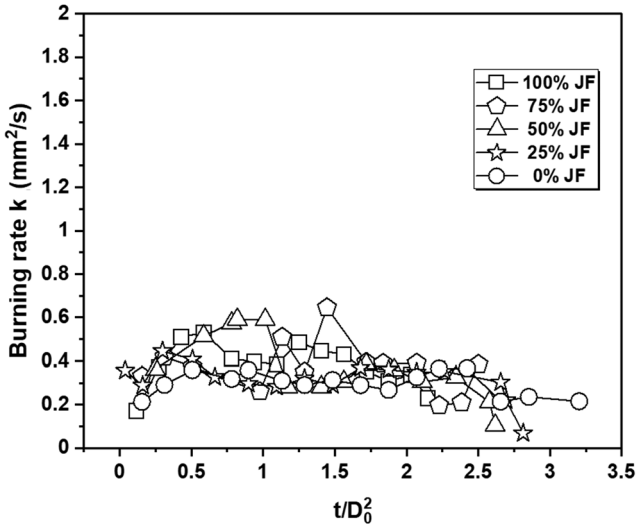

Figure 13. Droplet burning rate as a function of the normalized time at 900 °C.

its burning rate until the lifetime of the droplet. The droplets with 75% Jet A-1 present a distinct behavior as a result of the occurrence of puffing and microexplosions (Figure 11), which enhances their burning rate k and shortens their lifetime. After the maximum value of k was reached, the 75% Jet A-1 D^2 curve displays a reduction in the slope at the later stages before the occurrence of microexplosions as a result of the expansions of inner gas bubbles before the breakup. These expansions occur as a result of the growth of inner gas bubbles that nucleate inside the fuel droplet.[12]

Figure 14 shows the global burning rates as a function of the air temperature. These global burning rates are obtained by

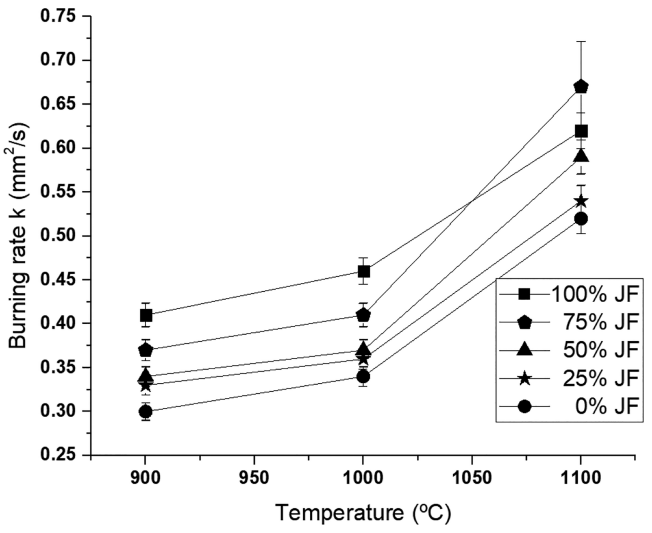

Figure 14. Global burning rates as a function of the temperature.

fitting the quasi-steady segments of the D^2-t curves to lines by least squares best fit. The quasi-steady segment was arbitrarily defined as the interval from D^2/D_0^2 = 0.9 to 0.2, excluding initial transient heating and later stages in droplet lifetime where the uncertainties become the order of magnitude of the size of the droplet. After that, a global burning rate was extracted for each test condition and each mixture. This way, the global effects of the blending agents in the different fuel mixtures can be compared between conditions. It can be stated that an increase in the ambient temperature leads to an increase in the burning rate and promotes the occurrence of disrupting burning phenomena for 75% Jet A-1 at the highest temperature. Thus, it can be theorized on the basis of the current literature that a further increase in the ambient temperature and ambient pressure would enhance the disruptive burning phenomena and even the occurrence for other fuel mixtures.[4,22] Additionally, when the percentage of Jet A-1 increases in the fuel mixture, the burning rate also tends to increase. The exception to this behavior occurs for the air temperature of 1100 °C, where the highest burning rate happens for the droplets with 75% Jet A-1. For this condition, secondary atomization in the form of puffing and microexplosion improved the burning characteristics of the fuel mixture, with the mixture being with secondary atomization, the mixture with the highest burning rate. It can also be concluded that fuels with higher aromatic contents (cf. Table 1) tend to have higher burning rates, which can be attributed to the higher volatility of the aromatic components and higher volatility of Jet A-1 seen in the distillation temperature differences. The effect of the volatility can also be noted through an earlier flame extinction in the mixtures with less jet fuel, leading to the conclusion that the composition of mixtures significantly affects the flame characteristics.

It is observed that the differences between the global burning rates of different fuels tend to be relatively insensitive to the temperature variation, except for 75% Jet A-1 and 50% Jet A-1. The former mixture presented a higher burning rate than the conventional jet fuel, and the latter mixture (which includes the maximum percentage of biofuel for a mixture accepted by the current legislation) presented a slightly lower burning rate than Jet A-1. When the ambient temperature was increased, 50% Jet A-1 presents an approximate burning rate to pure Jet A-1, highlighting the potential for using fuel mixtures to improve the burning performance of alternative fuels and promoting their further implementation in the aviation sector.

4. CONCLUSION

The present work evaluated the combustion of Jet A-1, HVO droplet, and their blends. The effect of a biofuel addition to a conventional jet fuel was investigated, and the main conclusions from this study can be summarized as follows. After ignition, a flame is established in the wake of each droplet for all test conditions. Flame intensity decreases and the droplet lifetime increases as the air temperature decreases, regardless of the composition of the fuel mixture. As the percentage of Jet A-1 in the fuel mixture increases, the flame intensity increases. The droplet diameter evolution follows the D^2 law for all conditions, except for the fuel mixture with 75% Jet A-1 at 1100 °C. The droplets of pure HVO present the longest burning time, and the droplets of pure Jet A-1 present the shortest burning time. The droplet burning time increases as the air temperature decreases.

The occurrence of puffing followed by microexplosions was observed for the fuel mixture with 75% Jet A-1. This phenomenon enhanced the burning rate and significantly reduced the droplet lifetime through the appearance of secondary atomization, highlighting the potential of this strategy for further implementation and improvement of the burning characteristics of alternative fuels in the aviation sector.

https://dx.doi.org/10.1021/acs.energyfuels.0c03476
Energy Fuels 2021, 35, 7232−7241

AUTHOR INFORMATION

Corresponding Author

Gonçalo Pacheco − *Instituto de Engenharia (IDMEC)–Laboratório Associado de Energia, Transportes e Aeronáutica (LAETA), Instituto Superior Técnico, Universidade de Lisboa, 1049-001 Lisboa, Portugal; Aeronautics and Astronautics Research Center (AEROG)–Laboratório Associado de Energia, Transportes e Aeronáutica (LAETA), Universidade da Beira Interior, 6201-001 Covilhã, Portugal;* orcid.org/0000-0002-2905-6230; Phone: +351218417186; Email: sousapacheco@tecnico.ulisboa.pt

Authors

André Silva − *Aeronautics and Astronautics Research Center (AEROG)–Laboratório Associado de Energia, Transportes e Aeronáutica (LAETA), Universidade da Beira Interior, 6201-001 Covilhã, Portugal;* orcid.org/0000-0002-4901-7140

Mário Costa − *Instituto de Engenharia (IDMEC)–Laboratório Associado de Energia, Transportes e Aeronáutica (LAETA), Instituto Superior Técnico, Universidade de Lisboa, 1049-001 Lisboa, Portugal;* orcid.org/0000-0002-3118-2762

Complete contact information is available at: https://pubs.acs.org/10.1021/acs.energyfuels.0c03476

Notes

The authors declare no competing financial interest.

ACKNOWLEDGMENTS

This work is dedicated to our dear supervisor, colleague, and friend, Prof. Mário Costa, who dedicated his life to research and education and transmitted to us his passion for the search of knowledge. The present work was performed under the scope of the LAETA activities, and it was supported by Fundação para a Ciência e Tecnologia (FCT) through the Projects UID/EMS/50022/2019 and UIDB/50022/2020.

REFERENCES

(1) International Air Transport Association (IATA). *IATA Sustainable Aviation Fuel Roadmap*; IATA: Montreal, Canada, 2015.

(2) Parker, R.; Lathoud, M. Green aero-engines: Technology to mitigate aviation impact on environment. *Proc. Inst. Mech. Eng., Part C* **2010**, *224*, 529−538.

(3) Kubičková, I.; Kubička, D. Utilization of triglycerides and related feedstocks for production of clean hydrocarbon fuels and petrochemicals: A review. *Waste Biomass Valorization* **2010**, *1*, 293−308.

(4) Lee, A.; Jiang, Y.; Zhu, D.; Law, C. Burning-Rate Enhancement of Organic Diazide Propellants: Dihalide Addition and Pressure Elevation. *AIAA J.* **1992**, *30*, 1298−1303.

(5) U.S. Department of Energy. *Alternative Aviation Fuels: Overview of Challenges, Opportunities, and Next Steps*; U.S. Department of Energy: Washington, D.C., 2007.

(6) Kandaramath Hari, T.; Yaakob, Z.; Binitha, N. N. Aviation biofuel from renewable resources: Routes, opportunities and challenges. *Renewable Sustainable Energy Rev.* **2015**, *42*, 1234−1244.

(7) Arvidsson, R.; Persson, S.; Fröling, M.; Svanström, M. Life cycle assessment of hydrotreated vegetable oil from rape, oil palm and Jatropha. *J. Cleaner Prod.* **2011**, *19*, 129−317.

(8) Neste Corporation. *Neste Renewable Diesel Handbook*; Neste Corporation: Espoo, Finland, 2015.

(9) Hileman, J. I.; Ortiz, D. S.; Bartis, J. T.; Wong, R.; Donohoo, P. E.; Weiss, M. A. *Near-Term Feasibility of Alternative Jet Fuels*; RAND Corporation: Santa Monica, CA, 2009.

(10) Gong, Y.; Kaario, O.; Tilli, A.; Larmi, M.; Tanner, F. X. A Computational Investigation of Hydrotreated Vegetable Oil Sprays Using RANS and a Modified Version of the RNG k-ϵ Model in OpenFOAM. *Proceedings of the SAE 2010 World Congress & Exhibition*; Detroit, MI, April 13−15, 2010; DOI: 10.4271/2010-01-0739.

(11) Botero, M. L.; Huang, Y.; Zhu, D.; Molina, A.; Law, C. K. Synergistic combustion of droplets of ethanol, diesel and biodiesel mixtures. *Fuel* **2012**, *94*, 342−347.

(12) Lapuerta, M.; Villajos, M.; Agudelo, J. R.; Boehman, A. L. Key properties and blending strategies of hydrotreated vegetable oil as biofuel for diesel engines. *Fuel Process. Technol.* **2011**, *92*, 2406−2411.

(13) Rahmes, T.; Kinder, J.; Crenfeldt, G.; LeDuc, G.; Abe, Y.; McCall, M.; Henry, T.; Zombanakis, G.; Lambert, D.; Lewis, C.; Andac, M; Juenger, J.; Reilly, K.; Holmgren, J.; Bozzano, A. Sustainable Bio-Derived Synthetic Paraffinic Kerosene (Bio-SPK) Jet Fuel Flights and Engine Tests Program Results. *Proceedings of the 9th AIAA Aviation Technology, Integration, and Operations Conference (ATIO)*; Hilton Head, SC, Sept 21−23, 2009; DOI: 10.2514/6.2009-7002.

(14) Law, C. Dryden Lecture: Fuel Options for Next Generation Chemical Propulsion. *Proceedings of the 49th AIAA Aerospace Sciences Meeting including the New Horizons Forum and Aerospace Exposition*; Orlando, FL, Jan 4−7, 2011; DOI: 10.2514/6.2011-1.

(15) Blakey, S.; Rye, L.; Wilson, C. W. Aviation gas turbine alternative fuels: A review. *Proc. Combust. Inst.* **2011**, *33*, 2863−2885.

(16) Schripp, T.; Herrmann, F.; Oßwald, P.; Kohler, M.; Zschocke, A.; Weigelt, D.; Mroch, M.; Werner-Spatz, C. Particle emissions of two unblended alternative jet fuels in a full scale jet engine. *Fuel* **2019**, *256*, 115903.

(17) Rao, D. C. K.; Karmakar, S.; Som, S. K. Puffing and micro-explosion behavior in combustion of butanol/Jet A-1 and acetone-butanol-ethanol (A-B-E)/Jet A-1 fuel droplets. *Combust. Sci. Technol.* **2017**, *189*, 1796−1812.

(18) Wang, C. H.; Liu, X. Q.; Law, C. K. Combustion and Microexpiosion of Freely Falling Multicomponent Droplets. *Combust. Flame* **1984**, *56*, 175−197.

(19) Ma, X.; Zhang, F.; Han, K.; Yang, B.; Song, G. Evaporation characteristics of acetone-butanol-ethanol and diesel blends droplets at high ambient temperatures. *Fuel* **2015**, *160*, 43−49.

(20) Armas, O.; Ballesteros, R.; Martos, F. J.; Agudelo, J. R. Characterization of light duty Diesel engine pollutant emissions using water-emulsified fuel. *Fuel* **2005**, *84*, 1011−1018.

(21) Megaritis, A.; Yap, D.; Wyszynski, M. L. Effect of water blending on bioethanol HCCI combustion with forced induction and residual gas trapping. *Energy* **2007**, *32*, 2396−2400.

(22) Rakopoulos, C. D.; Antonopoulos, K. A.; Rakopoulos, D. C. Experimental heat release analysis and emissions of a HSDI diesel engine fueled with ethanol-diesel fuel blends. *Energy* **2007**, *32*, 1791−1808.

(23) Shinjo, J.; Xia, J.; Ganippa, L. C.; Megaritis, A. Physics of puffing and microexplosion of emulsion fuel droplets. *Phys. Fluids* **2014**, *26*, 103302.

(24) Wang, C. H.; Law, C. K. Microexplosion of Fuel Droplets under High Pressure. *Combust. Flame* **1985**, *59* (1), 53−62.

(25) Wang, J.; Huang, X.; Qiao, X.; Ju, D.; Sun, C. Experimental study on effect of support fiber on fuel droplet vaporization at high temperatures. *Fuel* **2020**, *268*, 117407.

(26) Pizziol, B.; Costa, M.; Panão, M. O.; Silva, A. Multiple impinging jet air-assisted atomization. *Exp. Therm. Fluid Sci.* **2018**, *96*, 303−310.

(27) Law, C. K. Recent advances in droplet vaporization and combustion. *Prog. Energy Combust. Sci.* **1982**, *8* (3), 171−201.

(28) Shang, W.; Yang, S.; Xuan, T.; He, Z.; Cao, J. Experimental Studies on Combustion and Microexplosion Characteristics of *n*-Alkane Droplets. *Energy Fuels* **2020**, *34* (12), 16613−16623.

(29) Muelas, Á.; Remacha, P.; Martínez, A.; Ballester, J. Combustion characteristics of isolated free-falling droplets of Jet A blended with ethanol and butanol. *Proceedings of the ASME Turbo Expo 2018: Turbomachinery Technical Conference and Exposition*; Lillestrøm, Norway, June 11−15, 2018; V04AT04A073.

https://dx.doi.org/10.1021/acs.energyfuels.0c03476
Energy Fuels 2021, 35, 7232−7241